Vertically Aligned Carbon Nanotube Electrodes Directly Grown on a Glassy Carbon Electrode

Serin Park,[†] Dong-Won Park,[†,‡] Cheol-Soo Yang,[†] Kwang-Rok Kim,[§] Jun-Hyuk Kwak,[†] Hye-Mi So,[⊥] Chi Won Ahn,[⊥] Beom Soo Kim,[‡] Hyunju Chang,[†] and Jeong-O Lee[†,*]

[†]NanoBio Fusion Research Center, Korea Research Institute of Chemical Technology, Sinseongno 19, Yuseong-gu, Daejeon 305-343, Korea, [‡]Department of Chemical Engineering, Chungbuk National University, Chungbuk 361-763, Korea, [§]Bio-Organic Science Division, Korea Research Institute of Chemical Technology, Daejeon 305-343, Korea, and [⊥]National NanoFab Center, Daejeon 305-806, Korea

ABSTRACT Three-dimensional microelectrodes were fabricated using glassy carbon electrodes combined with vertically aligned carbon nanotubes (VACNTs). VACNTs were grown on various conducting electrode patterns including a carbon electrode fabricated by pyrolysis of a negative photoresist, with plasma-enhanced chemical vapor deposition using a bilayer Fe/Al catalyst. VACNT electrodes grown on the glassy carbon showed excellent electrochemical behavior, whereas VACNT electrodes grown on Pt showed poor electrochemical performance, presumably due to the poor contact between VACNTs and the Pt electrode. Electron microscopy showed that the VACNT layer was strongly bound to the carbon electrode, while that on Pt tended to peel away. The versatility of the all-carbon microelectrodes was also tested by using them for interfacing stem cells. Their superior mechanical properties and the electrical connectivity between the carbon electrode and the VACNTs, along with the simple fabrication process, suggest that glassy carbon may be a good conducting substrate for VACNT electrodes.

KEYWORDS: vertically aligned carbon nanotubes · electrode · pyrolysis · chemical vapor deposition

Vertically aligned carbon nanotubes (VACNTs) on metal substrates are useful in diverse applications that take advantage of the materials' three-dimensional properties and large surface area. These geometric advantages, combined with the excellent electrical properties of CNTs, could enable development of high-performance fuel cell electrodes and supercapacitors,[1−3] electron emitters, such as field emission devices,[4,5] interconnects,[6,7] and highly sensitive electrochemical sensors.[8] CNTs may be vertically aligned using molecular self-assembly[9] or conductive glues on a metallic substrate, although direct growth of CNTs on a metallic substrate may provide the most robust mechanical and electrical contacts. Until now, CNTs have mainly been grown on insulating substrates, such as SiO_2 or sapphire. Transition metal catalysts have not been used with conducting substrates because they tend to form alloys with substrates at the relevant growth temperatures or they coarsen and segregate during growth.[10,11] Conducting substrates with high melting (alloying) temperatures are good substrate candidates for growing CNTs directly. Thin insulating layers, such as Al_2O_3, may be used as a buffer layer to stop the poisoning of catalyst particles. Insulating layers, however, cannot provide an electrical connection to the conducting substrate, and additional fabrication processes are required for formation of electrical contacts with the substrate. Recently, Talapatra and colleagues succeeded in growing CNTs directly on Inconel 600 using vapor pressure catalyst delivery.[12] In this case, the catalyst was delivered as a vapor so that it was not poisoned by alloying with the substrate. Although robust VACNTs on metallic substrates may be produced using this technique, it cannot be applied to patterned growth approaches that are critical for many applications. Nessim *et al.* succeeded in growing VACNTs directly on Ta substrates at low temperatures,[13] relying on the fact that the rate-limiting step in CNT synthesis is the decomposition of the carbon feedstock.[13,14] In their work, they chose Ta as a substrate because of its high melting temperature. The carbon source was preheated before delivery to the substrate along with Fe. CNTs grown on TiN electrodes exhibited excellent electrochemical characteristics and were successfully employed for measuring cell signals.[15,16] Though CNTs grown on a TiN or Ta electrode showed superior characteristics, the process window for the fabrication of TiN or Ta is rather narrow.[11] CNT electrodes could be further improved by employing a simple fabrication process and aligning CNTs better.

Here, we report the fabrication of VACNT electrodes directly grown on conducting films using plasma-enhanced chemical vapor deposition (PECVD). An Al/Fe bilayer was

* Address correspondence to jolee@krict.re.kr.

Received for review May 16, 2011 and accepted August 14, 2011.

Published online August 15, 2011
10.1021/nn2017815

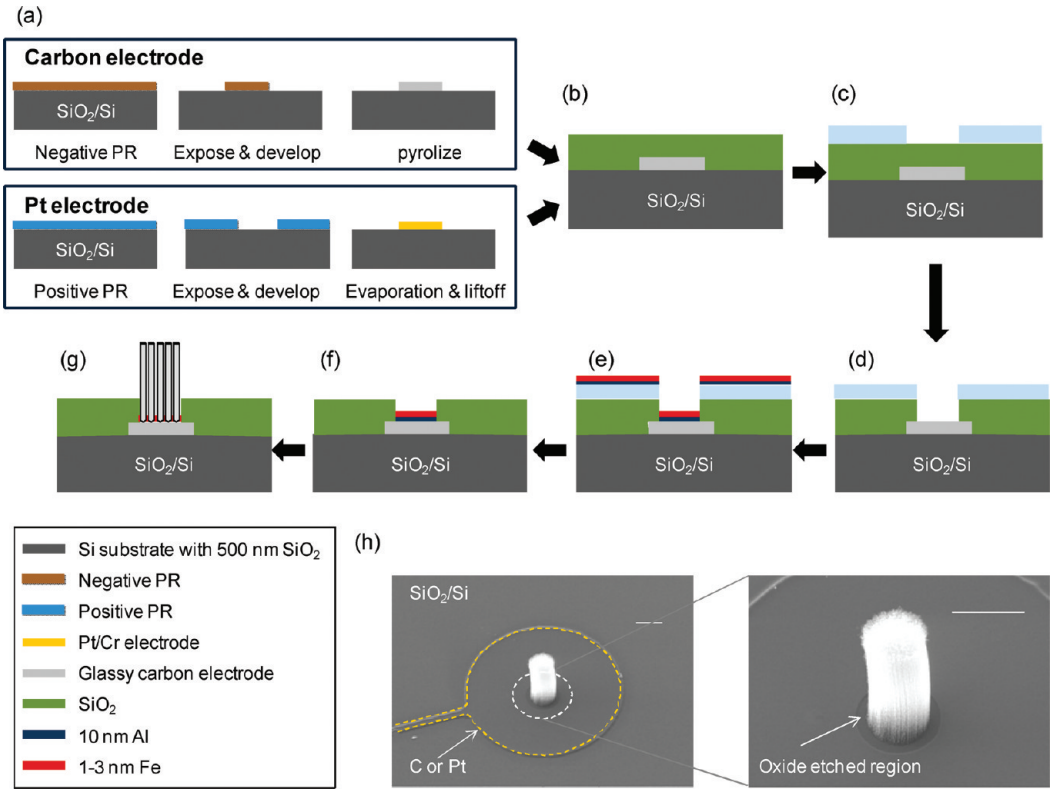

Figure 1. Schematics of sample fabrication process. (a) Fabrication of metal or carbon electrode using photolithography. (b) Insulation of the entire surface with 200 nm thick SiO_2 (green). (c) Opening windows for catalyst deposition and external contact using photolithography (light blue; patterned photoresist). (d) Selective etching of SiO_2 using buffered oxide etcher (BOE). (e) Evaporation of catalyst layer (10 nm Al {dark blue} followed by 1−3 nm Fe {red}). (f) Lift-off. (g) Growth of VACNTs. (h) Representative image of a VACNT electrode fabricated with the above process sequence. Yellow dashed lines indicate bottom disk electrode fabricated with metal evaporation or pyrolysis of photoresists. As shown in the enlarged SEM image on the right side, entire sample was coated with 200 nm thick SiO_2 except for VACNTs. Scale bar: 10 μm.

used as a catalyst layer, and the thickness of the Al exceeded 10 nm to ensure an electrical connection with the metallic substrate. Two conducting electrodes were demonstrated to provide conducting supports for the VACNT electrodes: glassy carbon and Pt. Although the glassy carbon electrodes with VACNTs showed excellent electrochemical behavior, the Pt electrodes with VACNTs exhibited poor electrochemical performance due to unstable mechanical contact between the VACNT layer and Pt. Electron microscopy analysis revealed that the interface between Pt and the VACNT layer was not mechanically robust, whereas the interface between carbon and the VACNTs was characterized by firm adhesion.

RESULTS AND DISCUSSION

Figure1 shows a schematic diagram of the sample preparation process. Standard photolithography and lift-off were used to fabricate Pt bottom electrodes, and the electrode patterns made with negative photoresist were pyrolyzed to yield glassy carbon electrode. Details regarding sample fabrication are given in the Materials and Methods section. After the conducting electrode formation, the bilayer of Fe/Al was used as a catalyst to grow VACNTs. We found that the presence of Al is prerequisite to grow CNTs on a conducting substrate; CNTs do not grow from Fe thin films deposited directly on pyrolyzed photoresist, metal electrode, or polymer patterns. Figure 1h shows a typical SEM image of a VACNT electrode. As shown in the image, only VACNTs are exposed and may form conducting paths since all other parts were insulated with 200 nm thick SiO_2. Supporting Information Figure S1 shows a high-resolution TEM image of VACNTs directly grown on a glassy carbon electrode. VACNTs are multiwall carbon nanotubes with a 10−20 nm diameter and ~10 walls maximum. Catalyst nanoparticles are on the tips of CNTs for thinner tubes, as shown in the Supporting Information Figure S1, but thick tubes or branched ones have catalyst particles on their stem.

Since we used Al as a buffer layer to prevent the poisoning of the catalyst, concerns may arise regarding the poor electrical conductance due to the presence of oxidized Al. Considering our fabrication conditions and processes, catalyst deposition in a high-vacuum environment, and oxygen-free, low-pressure CVD growth of CNTs, it would be rather difficult to observe the effects of barriers in electrical conduction due to the oxidized Al. To check the electrical connection between VACNTs and bottom electrode patterns, we measured two-probe conductance in between VACNTs and the

bottom electrode and analyzed the state of Al using X-ray photoemission spectroscopy (XPS). Figure 2 shows *I*−*V* characteristics measured between VACNTs and the glassy carbon electrode. The inset shows a schematic of the measurement layout. For electrical characterization, samples with a large (~1 mm^2) VACNT area were fabricated on both glassy carbon and Pt electrodes. Because we used silver paste with very high viscosity, we could safely rule out the possibility of diffused silver paste making direct contact with the bottom electrode.

In Figure 2, showing linear *I*−*V* characteristics observed between VACNTs and the carbon electrode, VACNTs and the carbon electrode have ohmic contact. Interestingly, the two-terminal resistance between VACNTs and the carbon electrode is much smaller than that of the carbon electrode itself. One may speculate that the contact resistance between the silver paste and glassy carbon is larger than the total sum of contact resistance between the silver paint and VACNTs, the resistance of VACNTs themselves, and contact resistance between VACNTs and the glassy carbon electrode. It has been reported that pyrolyzed polymer films are unstable in air; the O/C ratio tripled with 100 h exposure in lab air.[17] Such an oxidized carbon surface could have contributed to the observed large contact resistance between the silver paste and the carbon electrode. Also, the fact that a glassy carbon surface normally requires "activation" to achieve an electrochemically active surface[18] could be correlated with the poor contact resistance between the silver paste and bare glassy carbon. *I*−*V* characteristics measured between VACNTs and Pt also show linear behavior (data not shown), though two-terminal resistance beween VACNTs and Pt is much larger than that of Pt itself. While two-probe resistance of the glassy carbon itself is around 1.65 kΩ, that of VACNTs and glassy carbon is about 600−750 Ω. In the case of Pt, two-probe resistance of the Pt itself was about 60−110 Ω, while 120−1.5 kΩ resistance was measured between VACNTs and Pt. Two-probe resistances between Pt and VACNTs show a sharp increase with a decrease in the VACNTs area. Although the XPS spectrum in Supporting Information Figure S2 shows the presence of oxidized Al in our sample, the *I*−*V* measurement confirms that the presence of oxidized Al does not hinder the electrical connection between VACNTs and the bottom electrode.

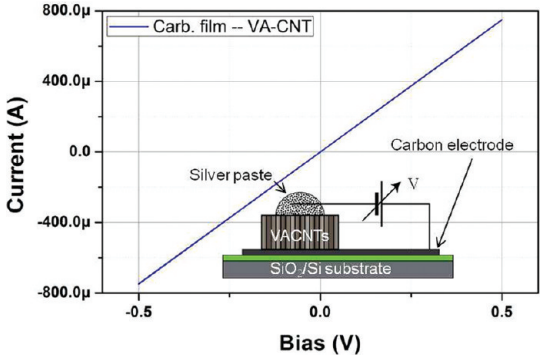

Figure 2. Two-probe conductance measurements between VACNTs and a glassy carbon electrode. All the measurement parameters were kept constant as much as possible. The inset shows a schematic of the measurement system.

Then, we characterized VACNT electrodes with electrochemical methods. Figure 3 compares the cyclic voltammograms (CV) measured from the glassy carbon with VACNTs and the Pt electrodes with VACNTs. CVs were measured with a Pt counter electrode and Ag/AgCl as a reference electrode. The insets of Figures 3a and b show scanning electron microscope (SEM) images

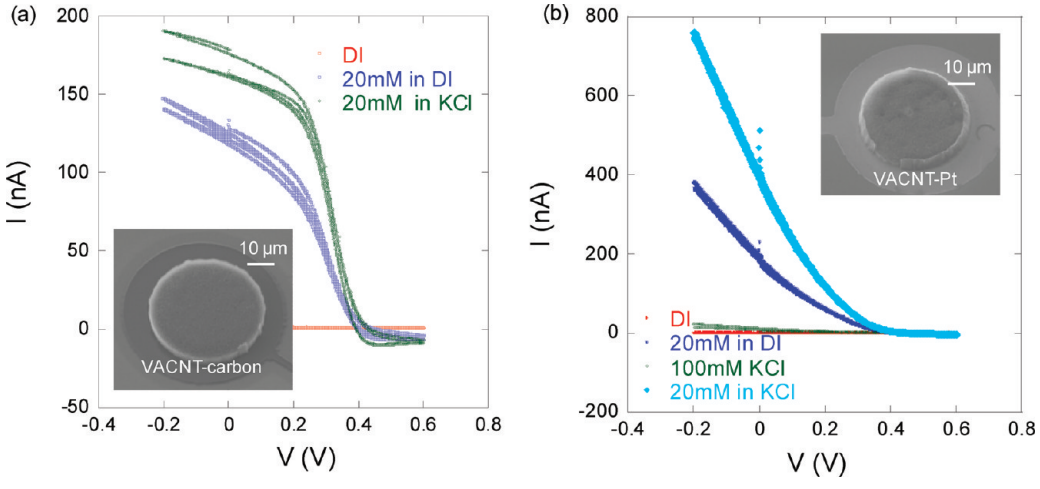

Figure 3. Electrochemical characteristics of the VACNT electrode. We used a Pt counter electrode and a Ag/AgCl reference electrode, and the scan rate was fixed as 50 mV/s. (a) Electrochemical characteristics of a VACNT electrode with a glassy carbon bottom electrode. The blue curve corresponds to 20 mM $K_3[Fe(CN)_6]$ in deionized (DI) water, and the green curve corresponds to 20 mM $K_3[Fe(CN)_6]$ in 100 mM KCl. The inset shows an SEM image of the device being measured. (b) Electrochemical characteristics of a VACNTs electrode on Pt. The blue curve corresponds to 20 mM $K_3[Fe(CN)_6]$ in DI water, and the cyan curve corresponds to 20 mM $K_3[Fe(CN)_6]$ in 100 mM KCl. The red curve and green curve correspond to the cyclic voltammogram of DI water and 100 mM KCl, respectively. The inset shows an SEM image of a Pt electrode on which VACNTs were grown.

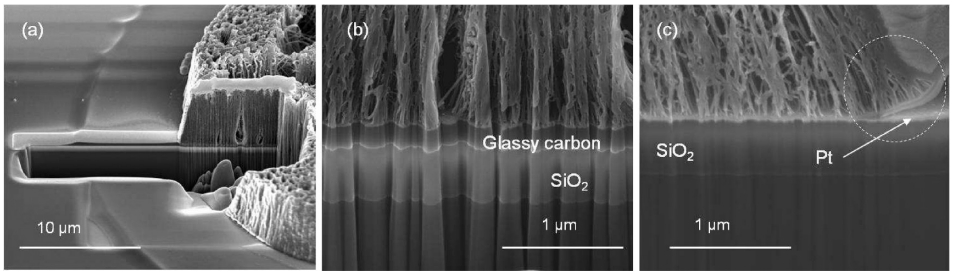

Figure 4. SEM images of the cross sections of VACNT grown carbon or Pt electrodes. All samples were coated with a thick Pt layer for protection. (a) Tilted view of the sculpted sample imaged after FIB. This particular sample is a glassy carbon electrode with VACNTs. The preparation of the sample for FIB is given in the Materials and Methods section. (b) Cross sectional view of the VACNTs grown on a glassy carbon electrode. The fiber-like structures found in the image are artifacts from FIB, possibly coming from local etch resistance of VACNTs. Similar artifacts were also found in VACNTs directly grown on Pt. (c) Cross sectional view of the VACNTs grown on a Pt electrode. At the right side of the image, highlighted with a dashed circle, the VACNT layer exfoliates from Pt.

of VACNT on glassy carbon electrodes and Pt electrodes, respectively.

As shown in the SEM images, high-density VACNTs were grown on conducting substrates. VACNTs were grown at 600 °C, 800 mTorr, using 100 sccm CH_4 as a carbon source. We used 1 nm thick Fe films on 10 nm thick Al as a catalyst for these samples, and the growth was carried out for 10 min with 320 W, 13.75 MHz RF plasma. Under the same process conditions, VACNTs grown on the carbon electrode looked very similar to those grown on a Pt electrode. They were mostly small-diameter multiwall CNTs with 10−20 nm diameter or double-wall CNTs of 2−3 μm in length. Although they looked very similar, the electrochemical properties of the carbon electrode were dramatically different from those of the Pt electrode. As shown in Figure 3a, $[Fe(CN)_6]^{3-}$ ions in solution will be oxidized to $[Fe(CN)_6]^{4-}$ with positive scan (heading toward the positive direction) using a VACNT−carbon electrode, and the faradaic current saturates around ~0.4 V. In the reverse direction, $[Fe(CN)_6]^{4-}$ ions are reduced back to $[Fe(CN)_6]^{3-}$. For a planar electrode, the current decreases after passing the peak potential, due to the consumption of oxidized (reduced) species, resulting in typical peak-shaped current−voltage characteristics. However, no decrease of current was observed in Figure 3a. Such a behavior is common for microelectrodes, since analytes diffuse with hemispherical diffusion in microelectrodes, leading to a higher mass transport per unit electrode surface.[19] The size of the VACNT disk was about 40 μm diameter, and the voltage separation between current peaks, ΔE_p in the cyclic voltammogram, was about 200 mV, comparable to the value reported by Fung *et al.*[16] The charge transfer kinetics of this system was relatively slow, partly because of the high resistivity of the glassy carbon electrode and the lack of oxygen functional groups at the electrode surfaces.[20] The conductivity of the glassy carbon film (250 nm thick) annealed at 900 °C was around 10−15 S/cm, and it should be possible to further improve the conductivity by optimizing the annealing conditions or doping the polymer films before pyrolysis.

Recently, pyrolyzed photoresists are emerging as new materials for conducting electrodes due to their ease of manufacturing, and they could provide robust contact for nanostructures. For example, Bonifas and McCreery used pyrolyzed photoresist films as electrodes for molecular devices,[21] and Cheng and colleagues fabricated ZnO nanowire arrays directly from pyrolyzed photoresists to yield ZnO array electrodes.[22] On the other hand, the Pt electrodes with VACNTs showed a higher current, but no clear reduction or oxidation peaks has observed. It is possible that the observed current is a combination of the faradaic current with charging current and other residual currents. Such poor reaction characteristics suggest that there could be a huge source of *iR* drop in this geometry: the VACNTs and the Pt are electrically or mechanically separated.

The interface between the VACNTs and the contact electrodes was examined by sculpting samples using a focused ion beam (FIB) and imaging the cross sections of the devices. Figure 4 compares SEM images of the interfaces between VACNTs and glassy carbon (Figure 4b) and Pt (Figure 4c), respectively.

As shown in Figure 4, whereas VACNTs bound firmly to the glassy carbon electrode pyrolyzed from photoresist, the VACNT layer exfoliated from the Pt electrode surface. Because the VACNT layer was grown using a Fe/Al bilayer, the interface between the Pt and Al was subjected to high temperatures during VACNT growth. Pt and Al form an intermetallic material at elevated temperatures,[23] which is brittle and possesses poor adhesion properties due to the stresses imposed during annealing. Interestingly, even in the presence of the Fe/Al bilayer catalyst, VACNTs only grew on the carbon and Pt electrodes; they were not observed to grow on Au or Cr electrodes. To confirm that the electrochemical signal measured using the glassy carbon electrode indeed came from the VACNTs, we decorated Au nanoparticles on the electrodes by electrochemical deposition. We again used cyclic voltammetry to decorate Au nanoparticles, and the potential was cycled

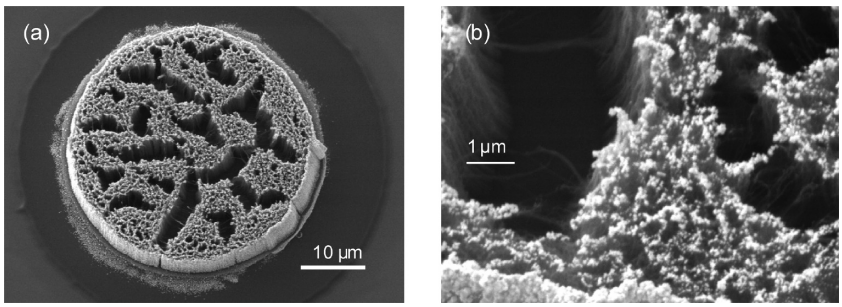

Figure 5. SEM images after Au decoration. (a) Glassy carbon disk electrode with VACNTs after Au decoration. (b) Magnified SEM image of a Au-decorated, VACNT-grown glassy carbon electrode. Most of the Au particles were found on the tips of the CNTs, and almost no Au particles were present at the bottom on the glassy carbon electrode surface.

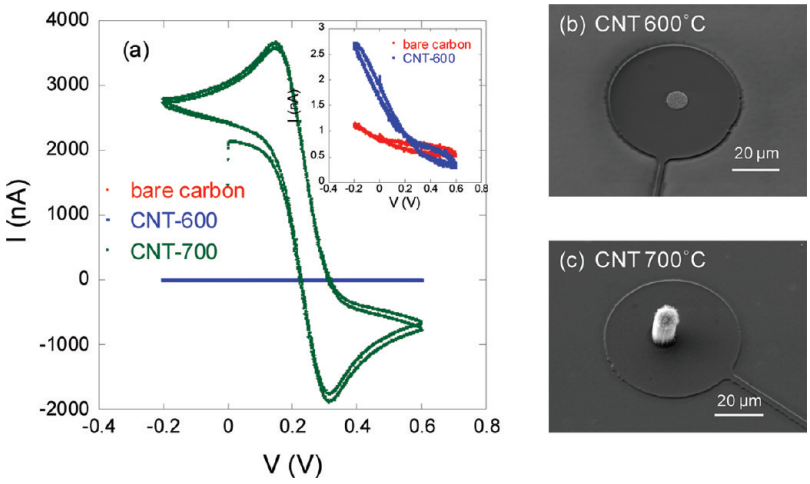

Figure 6. Effect of synthesis temperature on the electrochemical characteristics of the microelectrodes. (a) Cyclic voltammograms measured with bare carbon (red), a carbon electrode with CNTs grown at 600 °C (blue), and a carbon electrode with VACNTs grown at 700 °C (green). The insets compare the cyclic voltammograms of a bare carbon electrode and a carbon electrode with CNTs grown at 600 °C. The redox-active species was provided by 20 mM $K_3[Fe(CN)_6]$ in PBS solution, and the scan rated was 50 mV/s. (b) SEM image of a glassy carbon electrode with CNTs grown at 600 °C. (c) SEM image of a glassy carbon electrode with CNTs grown at 700 °C.

from −1 to 1 V in 50 μM $HAuCl_4$ with a Ag/AgCl reference electrode and Pt wire as the counter electrode. Figure 5 shows SEM images of the carbon disk electrodes with VACNTs after decoration with Au nanoparticles.

As shown in Figure 5a, VACNTs formed smaller sized bundles after decoration. A similar effect was observed in vertically aligned arrays of nanorods or CNTs, and the driving force was explained by the capillary force originating from narrow nanochannels between high aspect ratio nanostructures.[24−27] Figure 5b shows an SEM image of the Au-decorated VACNT electrode under high magnification. As is clear from the image, Au nanoparticles were mostly present on the tips of the CNTs, and almost no Au nanoparticles were found on the glassy carbon bottom electrode surfaces. We performed the same experiments with longer tubes; uniform-sized Au nanoparticles were decorated on the tips of VACNTs as well as on the sidewalls (Supporting Information Figure S3). These results confirm that we successfully fabricated VACNT electrodes and that the tips of the VACNTs as well as outermost sidewalls of VACNTs were the most chemically active regions in reduction of Au ions.[28] We also decorated Au nanoparticles on VACNT electrodes directly grown on Pt electrodes. Unlike the case of VACNT−glassy carbon electrodes, only a few large Au nanoparticles were found on VACNT−Pt electrodes, as shown in the Supporting Information Figure S4, and some particles were formed on the SiO_2 layer where oxide leaks.

Because we showed that glassy carbon electrodes with VACNTs exhibited superior electrochemical properties compared with the Pt electrode, we further investigated the properties of the glassy carbon electrodes with VACNTs. As the synthesis temperature increased, the number of CNT defects decreased, and one would expect that electrodes with VACNTs grown at higher temperatures would perform better. Figure 6 shows a comparison of the electrochemical signals from a bare glassy carbon electrode, a glassy carbon electrode with VACNTs grown at 600 °C, and a glassy carbon electrode with VACNTs grown at 700 °C. The thickness of the Fe film that was used as a catalyst was 3 nm, and all process conditions were identical except for the synthesis temperature. Figure 6a shows the

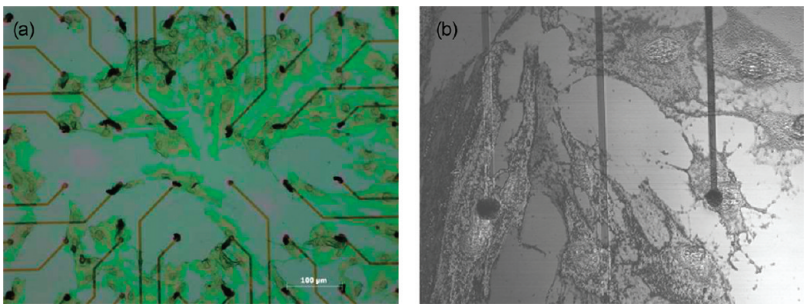

Figure 7. MEA fabricated with glassy carbon–VACNT electrodes. (a) Optical micrograph of the VACNT MEAs with rat BMSCs. (b) Confocal micrograph of the VACNT MEAs. Dark spots correspond to VACNTs. The image was taken with 488 nm excitation.

cyclic voltammograms from those three devices with $K_3[Fe(CN)_6]$ as a redox-active species in phosphate-buffered saline (PBS) solution. As shown in the SEM images in Figure 6b, CNTs grown at 600 °C with a 3 nm thick Fe catalyst exhibited short (<1 μm), tangled, thicket-like morphologies. On the other hand, CNTs grown at 700 °C were vertically aligned with a high density and lengths longer than 10 μm. Supporting Information Figure S5 compares the transmission electron microscopy (TEM) images of VACNTs grown at 600 °C with those of VACNTs grown at 700 °C. The electrochemical characteristics of glassy carbon electrodes with VACNTs changed dramatically with the synthesis temperature. As shown in the inset of Figure 6a, bare carbon electrodes themselves showed very poor electrochemical characteristics, and CNTs grown at 600 °C improved the performance only slightly. However, VACNTs grown at 700 °C yielded clear electrochemical signals that were 10^3 times greater than those of the bare carbon electrode or electrode with VACNTs grown at 600 °C. The electrochemical signals measured were far greater than the values measured from Au electrodes of comparable size (Supporting Information Figure S6). To confirm such an enhancement is indeed coming from VACNTs, we processed the glassy carbon electrode in VACNTs growth conditions without catalyst. About 10% increase in conductivity was observed in glassy carbon electrodes processed in VACNT growth conditions, which is far too small to account for the increase in electrochemical signals we observed.

Finally, we demonstrated the versatility of VACNT electrodes by applying them to multielectrode arrays (MEA) for extracellular signal measurement. As was reported previously,[29–31] CNTs facilitate the adhesion and proliferation of cells. As a model system, we chose rat bone marrow stem cells (BMSCs) and induced them to differentiate to neuronal cells. Details regarding cell preparation are discussed in the Materials and Methods section. Figure 7 shows optical microscopy images of VACNT MEAs with BMSCs; cells prefer to adhere directly on top of VACNTs, while considerably fewer numbers of cells are found on a commercial TiN electrode under the same conditions (data not shown). Also, cells exhibit an excellent affinity to VACNTs; cells strongly adhere to VACNTs, or VACNTs are completely encapsulated by cell bodies, as shown in the SEM image in Supporting Information Figure S7.

CONCLUSIONS

We produced VACNTs on conducting substrates using an Fe/Al bilayer as the catalyst. Among the various conducting substrates tested, carbon electrodes fabricated by pyrolysis of a negative photoresist exhibited excellent compatibility with VACNTs. Even though XPS analysis revealed the presence of oxidized Al between VACNTs and the carbon electrode, ohmic *I–V* characteristics were observed between VACNTs and the carbon electrode. For a better understanding regarding the origin of oxidized Al and its role on the fabrication and electrical characteristics of VACNT electrodes, further work should be done including *in situ* XPS analysis. Microscopy revealed that the VACNT–carbon electrodes possessed better binding affinity than the VACNT–Pt electrodes. High-performance three-dimensional electrodes could be fabricated using this approach, and possible applications to electrochemical sensors and electrophysiology probes were demonstrated. The simple fabrication process and excellent electrochemical characteristics suggest that carbon electrodes made by the pyrolysis of polymers are ideal conducting substrates for growing VACNTs directly, and this all-carbon approach may be applied to high-performance electrochemical sensors, electron emission devices, and prosthetic devices for *in vivo* signal measurements.[32]

MATERIALS AND METHODS

Fabrication of VACNT Electrodes. Fabrication of the VACNT electrodes proceeded in three steps: bottom electrode formation, insulation and catalyst patterning, and CNT growth. VACNTs with metal electrodes were fabricated by using photolithography and lift-off. We used positive photoresists (a bilayer of PMGI (polymethylglutarimide) and GXR601, Microchem, Newton, MA, USA) on silicon substrates with 500 nm thermal oxide.

The electrode metals were then deposited using e-beam evaporation with a thin layer of a Cr (3 nm) buffer layer. Deposition of a Cr buffer layer is necessary in order to enhance the adhesion of Pt on the SiO_2 surface. Pt electrode patterns were completed by lift-off in 80 °C heated Remover PG (Microchem, Newton, MA, USA). To fabricate the carbon bottom electrode, we used commercially available SU8-2002 negative photoresists (Microchem, Newton, MA, USA), which are widely used to produce structures with high aspect ratios.[33] After making patterns with SU8 resists on a Si substrate with 500 nm SiO_2, samples were annealed in vacuum at 900 °C for 30 min. The thickness of the resist decreased from 2 μm to ~250 nm after annealing, providing a smooth surface (Supporting Information, Figure S8). The resistivities of the pyrolyzed SU resist decreased with increasing annealing temperature and annealing time. Pyrolyzed polymer films result in a glassy carbon that can withstand high temperatures. It is chemically stable and has a low porosity and permeability. Glassy carbon is widely used as an electrode material in electrochemistry, in high-temperature crucibles, and as a component of prosthetic devices.[34,35] After bottom electrode patterning, the entire sample was coated with SiO_2 (200 nm) for insulation using low stress PECVD (at 350 °C, 1200 mTorr, with 75 sccm SiH_4 and 3300 sccm N_2O. The deposition time for 200 nm oxide was 48 s). Then, patterns for the electrode contacts and catalyst position were introduced on the top layer. Insulating layers were selectively removed by wet etching with buffered oxide etcher. Without removing the photoresist patterns, a bilayer of 10 nm Al and 1−3 nm Fe was evaporated as a catalyst layer. First Al and then Fe layers were evaporated successively without breaking the vacuum, and in order to prevent the oxidation of Al, and the base pressure of the evaporation chamber was kept below 2×10^{-6} Torr. There is AlO_x present in our VACNT electrodes, as shown in the XPS images in Supporting Information Figure S2. However, we confirmed that they did not affect the electrical connection between VACNTs and the Pt or C electrode significantly, by measuring the conductance between the glassy carbon electrode (Pt electrode) and the VACNTs. It is possible that Al was oxidized after VACNT growth. After lift-off, samples were transferred to a 4 in. PECVD to carry out nanotube growth. VACNTs were grown at 600−700 °C for 10 min with 100 sccm CH_4 as a carbon source. A small amount of hydrogen (10 sccm) could be introduced in the chamber while heating or growing CNTs, but the effect of hydrogen is not dramatic. Without H_2, more amorphous carbon layers were formed at the outer walls of the CNTs. To facilitate the growth of VACNTs, the pressure of the process chamber was kept at 800 mTorr, with 320 W, 13.75 MHz RF plasma. Figure 1 shows a schematic diagram of the sample fabrication process and SEM images of VACNT electrodes.

Sample Preparation for Investigating Microscopic Interfaces. To investigate the interface between the VACNTs and the contact electrodes, samples were micromachined using a focused ion beam (Helios Nanolab, FEI company). The ion beam was tilted 52° with respect to the electron beam and was used only for milling. The VACNTs on the electrode were milled with a Ga^+ ion beam current of 6.5 nA with the acceleration voltage of 30 keV.

Electrochemical Characterizations. For electrochemical characterizations, we used $K_3[Fe(CN)_6]$ as the redox-active species either in DI water, 100 mM KCl, or phosphate-buffered saline solution as supporting electrolyte. Samples were encased in a liquid cell made with plexiglass, which can hold ~500 μL of solution. VACNT electrodes were used as working electrodes, and cyclic voltammetry was performed with a Ag/AgCl reference electrode and a Pt wire in the solution as counter electrode. The scan rate was fixed as 50 mV/s unless specified with other scan rates. For decoration of Au nanoparticles, we prepared 100 μM $HAuCl_4$ in PBS solution and performed cyclic voltammetry from −1 to 1 V.

Cell Preparation and Growth. Rat bone marrow stem cells were obtained from femurs of adult male Fisher rats as described previously[36] and maintained in the DMEM medium (Hyclone) supplemented with 10% FBS (Gibco), 100 units/mL penicillin, and 100 μg/mL streptomycin (Gibco). The nonadherent cells were removed after 48 h and the adherent remained. BMSCs were washed twice with fresh medium. The cells were then continuously cultured for 10 days. The media was changed each 3 days. The cultured cells were seeded at five passages by 1×10^5/mL on the MEA culture chamber. To induce the neuronal differentiation, we treated 20 μM compound **1** in the seeded cells.[37] After 2 days, we checked the extracellular potential of the neuronal differentiated cells with MEA systems (MCS GmbH, Reutlingen, Germany), and cell morphologies with a confocal microscope (LSM5 Exiter, Zeiss, Jena, Germany). For scanning microscope images, cells bound with VACNT MEA were dried with graded alcohol and imaged using a Mira XII field emission microscope (Tescan, Czech republic).

Acknowledgment. Financial support from the Korea Research Council for Industrial Science and Technology, National Research Foundation (NRF, No. K20722000002-09B0100-00210), and "The Support Program for the Advancement of National Research Facilities and Equipment" of the Korean government are gratefully acknowledged.

Supporting Information Available: High-resolution TEM image of VACNTs, XPS measured from VACNT electrodes on glassy carbon, SEM images of Au-decorated VACNTs on glassy carbon, SEM image of a Au-decorated VACNT on a Pt electrode, TEM images of VACNTs grown at 600 and 700 °C, electrochemical signals from 10 μm diameter Au microelectrode, FESEM images of VACNT MEAs, and AFM images of the pyrolyzed SU8 film. These materials are available free of charge *via* the Internet at http://pubs.acs.org.

REFERENCES AND NOTES

1. Gong, K.; Du, F.; Xiz, Z.; Durstock, M.; Da,i, L. Nitrogen-Doped Carbon Nanotube Arrays with High Electrocatalytic Activity for Oxygen Reduction. *Science* **2009**, *323*, 760–764.
2. Futaba, D. N.; Hata, K.; Yamada, T.; Hiraoka, T.; Hayamizu, Y.; Kakudate, Y.; Tnaike, O.; Hatori, H.; Yumura, M.; Ijima, S. Shape-Engineerable and Highly Densely Packed Single-Walled Carbon Nanotubes and Their Application as Super-Capacitor Electrodes. *Nat. Mater.* **2006**, *5*, 987–994.
3. Lu, W.; Qu, L. T.; Henry, K.; Dai, L. M. High Performance Electrochemical Capacitors from Aligned Carbon Nanotube Electrodes and Ionic Liquid Electrolytes. *J. Power Sources* **2009**, *189*, 1270–1277.
4. Minoux, E.; Groening, O.; Teo, K. B. K.; Dalal, S. H.; Gangloff, L.; Schnell, J. P.; Hudanski, L.; Bu, I. Y. Y; Vincent, P.; Legagneux, P.; *et al*. Achieving High-Current Carbon Nanotube Emitters. *Nano Lett.* **2005**, *5*, 2135–2138.
5. Modi, A.; Koratkar, N.; Lass, E.; Wei, B.; Ajayan, P. M. Miniaturized Gas Ionization Sensors Using Carbon Nanotubes. *Nature* **2003**, *424*, 171–174.
6. Esconjauregui, S.; Fouquet, M.; Bayer, B. C.; Ducati, C.; Smajda, R.; Hofmann, S.; Robertson, J. Growth of Ultrahigh Density Vertically Aligned Carbon Nanotube Forests for Interconnects. *ACS Nano* **2010**, *4*, 7431–7436.
7. Zhang, C.; Yan, F.; Allen, C. S.; Bayer, B. C.; Hofmann, S.; Hickey, B. J.; Cott, D.; Zhong, G.; Robertson, J. Growth of Vertically-Aligned Carbon Nanotube Forests on Conductive Cobalt Disilicide Support. *J. Appl. Phys.* **2010**, *108*, 024311.
8. Ahammad, A. J. S.; Lee, J. J.; Rahman, M. A. Electrochemical Sensors Based on Carbon Nanotubes. *Sensors* **2009**, *9*, 2289–2319.
9. Diao, P.; Liu, Z. Vertically Aligned Single-Walled Carbon Nanotubes by Chemical Assembly - Methodology, Properties, and Applications. *Adv. Mater.* **2010**, *22*, 1430–1449.
10. Nessim, G. D.; Acquaviva, D.; Seita, M.; O'Brien, K. P.; Thompson, C. V. The Critical Role of the Underlayer Material and Thickness in Growing Vertically Aligned Carbon Nanotubes and Nanofibers on Metallic Substrates by Chemical Vapor Deposition. *Adv. Funct. Mater.* **2010**, *20*, 1306–1312.
11. Bayer, B. C.; Hofmann, S.; Castellarin-Cudia, C.; Blume, R.; Baehtz, C.; Esconjauregui, S.; Wirth, C. T.; Oliver, R. A.; Ducati, C.; Knop-Gericke, A.; *et al*. Support-Catalyst-Gas Interactions During Carbon Nanotube Growth on Metallic Ta Films. *J. Phys. Chem. C* **2011**, *115*, 4359–4369.

12. Talapatra, S.; Kar, S.; Pal, S. K.; Vajtai, R.; Ci, L.; Victor, P.; Shaijumon, M. M.; Kaur, S.; Nalamasu, O.; Ajayan, P. M. Direct Growth of Aligned Carbon Nanotubes on Bulk Metals. *Nat. Nanotechnol.* **2006**, *1*, 112–116.
13. Nessim, G. D.; Seita, M.; O'Brien, K. P.; Hart, A. J.; Bonaparte, R. K.; Mitchell, R. R.; Thomson, C. V. Low Temperature Synthesis of Vertically Aligned Carbon Nanotubes with Electrical Contact to Metallic Substrates Enabled by Thermal Decomposition of the Carbon Feedstock. *Nano Lett.* **2009**, *9*, 3398–3405.
14. Mora, E.; Pigos, J. M.; Ding, F.; Yakobson, B. I.; Harutyunyan, A. R. Low-Temperature Single-Wall Carbon Nanotubes Synthesis: Feedstock Decomposition Limited Growth. *J. Am. Chem. Soc.* **2008**, *130*, 11840–11841.
15. Gabay, T.; Ben-David, M.; Kalifa, I.; Sorkin, R.; Abrams, Z. R.; Ben-Jacob, E.; Hanein, Y. Electro-chemical and Biological Properties of Carbon Nanotube Based Multi-Electrode Arrays. *Nanotechnology* **2007**, *18*, 035201–035206.
16. Fung, A. O.; Tsiokos, C.; Paydar, O.; Chen, L. H.; Jin, S.; Wang, Y.; Judy, J. W. Electrochemical Properties and Myocyte Interaction of Carbon Nanotube Microelectrodes. *Nano Lett.* **2010**, *10*, 4321–4327.
17. Ranganathan, S.; McCreery, R. L. Electroanalytical Performance of Carbon Films with Near-Atomic Flatness. *Anal. Chem.* **2001**, *73*, 893–900.
18. McCreery, R. L. Advanced Carbon Electrode Materials for Molecular Electrochemistry. *Chem. Rev.* **2008**, *108*, 2646–2687.
19. Nirmaier, H.-P.; Henze, G. Characteristic Behavior of Macro-, Semimicro- and Microelectrodes in Voltammetric and Chronoamperometric Measurements. *Electroanalysis* **1997**, *9*, 619–624.
20. Hadi, M.; Rouhollahi, A.; Yousefi, M.; Taidy, F.; Malekfar, R. Electrochemical Characterization of a Pyrolytic Carbon Film Electrode and the Effect of Anodization. *Electroanalysis* **2006**, *18*, 787–792.
21. Bonifas, A. P.; LcCreery, R. L. `Soft' Au, Pt and Cu Contacts for Molecular Junctions Through Surface-Diffusion-Mediated Deposition. *Nat. Nanotechnol.* **2010**, *5*, 612–617.
22. Cheng, C.; Lei, M.; Wong, T. L.; Ho, K. M.; Fung, K. K.; Loy, M. M. T.; Yu, D.; Wang, N. High-Quality ZnO Nanowire Arrays Directly Fabricated from Photoresists. *ACS Nano* **2009**, *3*, 53–58.
23. Murarka, S. P.; Blech, I. A.; Levinstein, H. J. Thin-film Interaction in Aluminum and Platinum. *Appl. Phys.* **1976**, *47*, 5175–5181.
24. Fan, J. G.; Dyer, D.; Zhang, G.; Zhao, Y.-P. Nanocarpet Effect: Pattern Formation During the Wetting of Vertically Aligned Nanorod Arrays. *Nano Lett.* **2004**, *4*, 2133–2138.
25. Correa-Duarte, M. A.; Wagner, N.; Rojas-Chapana, J.; Morsczeck, C.; Thie, M.; Giersig, M. Fabrication and Biocompatibility of Carbon Nanotube-Based 3D Networks as Scafolds for Cell Seeding and Growth. *Nano Lett.* **2004**, *4*, 2233–2236.
26. Liu, H.; Li, S.; Zhai, J.; Li, H.; Zheng, Q.; Jiang, L.; Zhu, D. Self-Assembly of Large-Scale Micropatterns on Aligned Carbon Nanotube Films. *Angew. Chem., Int. Ed.* **2004**, *43*, 1146–1149.
27. Chakrapani, N.; Wei, B.; Carrillo, A.; Ajayan, P. M.; Kane, R. S. Capillary-Driven Assembly of Two-Dimensional Cellular Carbon Nanotube Foams. *Proc. Natl. Acad. Sci.* **2004**, *101*, 4009–4013.
28. Gong, K.; Chakrakarti, S.; Dai, L. Electrochemistry at Carbon Nanotube Electrodes: Is the Nanotube Tip More Active Than the Sidewall? *Angew. Chem., Int. Ed.* **2008**, *47*, 5446–5450.
29. Shein, M.; Greenbaum, A.; Gabay, T.; Sorkin, R.; David-Pur, M.; Hanein, Y. Engineered Neuronal Circuits Shaped and Interfaced with Carbon Nanotube Microelectrode Arrays. *Biomed. Microdevices.* **2009**, *11*, 495–501.
30. Lobo, A. O.; Corat, M. A. F.; Antunes, E. F.; Palma, M. B. S.; Pacheco-Soares, C.; Garcia, E. E.; Corat, E. J. An Evaluation of Cell Proliferation and Adhesion on Vertically-Aligned Multi-Walled Carbon Nanotube Films. *Carbon* **2010**, *48*, 245–254.
31. Zanello, L. P.; Zhao, B.; Hu, H.; Haddon, R. C. Bone Cell Proliferation on Carbon Nanotubes. *Nano Lett.* **2006**, *6*, 562–567.
32. Wallace, G. G.; Moulton, S. E.; Clark, G. M. Electrode-Cellular Interface. *Science* **2009**, *324*, 185–186.
33. Martinez-Duarte, R.; Gorkin, R. A., III; Abi-Samra, K.; Madou, M. J. The Integration of 3D Carbon-Electrode Dielectrophoresis on a CD-like Centrifugal Microfluidic Platform. *Lab Chip* **2010**, *10*, 1030–1043.
34. Cowlard, F. C.; Lewis, J. C. J. Vitreous Carbon—A New Form of Carbon. *Mater. Sci.* **1967**, *2*, 507–512.
35. Bokros, J. C. Carbon Biomedical Devices. *Carbon* **1977**, *15*, 355–371.
36. Rivera, F. J.; Sierralta, W. D.; Minguell, J. J.; Aigner, L. Adult Hippocampus Derived Soluble Factors Induce a Neuronal-Like Phenotype in Mesenchymal Stem Cells. *Neurosci. Lett.* **2006**, *406*, 49–54.
37. Kim, N. R.; Kang, S. K.; Ahn, H. H.; Kwon, S. W.; Park, W. S.; Kim, K. S.; Kim, S. S.; Jung, H. J.; Choi, S. U.; Ahn, J. H.; *et al.* Discovery of a New and Efficient Small Molecule for Neuronal Differentiation from Mesenchymal Stem Cell. *J. Med. Chem.* **2009**, *52*, 7931–7933.